ISSN: 2996 - 2498

Research Article

Environmental Science and Climate Research

Analyzing Variability of Rainfall and Meteorological Drought Over Wolaita Zone, Ethiopia

Adugna Arba Altaye[1,2*] and Abebe Kebede Habtegebriel[1]

[1]*Arba Minch University, Water Technology Institute, Faculty of Meteorology and Hydrology, Arba Minch, Ethiopia*

[2]*Ethiopian Meteorology Institute, Southern Regions Meteorological Service Research Center, Hawassa, Ethiopia*

[*]Corresponding Author
Adugna Arba Altaye, Arba Minch University, Water Technology Institute, Faculty of Meteorology and Hydrology, Arba Minch, Ethiopia.

Submitted: 2024, Nov 01; **Accepted:** 2024, Dec 09; **Published:** 2024, Dec 30

Citation: Altaye, A. A., Habtegebriel, A. K. (2024). Analyzing Variability of Rainfall and Meteorological Drought Over Wolaita Zone, Ethiopia. *Env Sci Climate Res, 2*(1), 01-15.

Abstract

Rainfall variability is one of the most significant climate variables for global agricultural productivity. It has also affected the agricultural activities, water and food security in the Wolaita Zone. Station and merged satellite data from 1990–2020 and data from the two stages of the Coupled Model Intercomparison Project (CMIP6) were used to analyze historical (1985–2014) and future projected meteorological drought changes from (2041–2100) via two shared socioeconomic pathways (SSPs) under the SSP2–4.5 and SSP5–8.5 emission scenarios. The variability in rainfall at the annual, seasonal, and monthly scales was analyzed by using the coefficient of variation (CV) and standardized rainfall anomalies (SRAs) across the study area. The modified Mann–Kendall test was used to determine the upward or downward trend and Sen's slope estimator was used to determine magnitude of increase or decrease. In this study, the power transformation (PT) bias correction method was used to correct the GCM (CMIP6) model data with the observed rainfall dataset serving as a reference. The SPI is the drought index, which indicates historical and future projected meteorological drought conditions at different severity levels that range from normal to extreme drought conditions. Future projected meteorological drought will be more affected by extreme and severe drought during the middle and far future under the SSP2–4.5 and SSP5–8.5 scenarios, which is more frequent and intense than the historical time over the study area. This study provides important guidance for identifying causes, minimizing impacts, and enhancing resilience to droughts in the Wolaita Zone.

Keywords: Wolaita Zone, Rainfall Variability, Trend, Meteorological Drought

1. Introduction

1.1. Background

Rainfall is one of the most significant climate variables for global agricultural productivity [1]. It is also a significant source of climate variability for East African countries, with extreme occurrences resulting in drought and heavy rainfall often associated with food, energy and water shortages; loss of life and property and many other socioeconomic impacts [2]. The economies of East African countries largely depend on agriculture, which is highly vulnerable to the amount and distribution of rainfall. Many researchers in regional and international studies have examined changes in rainfall variability due to recent climate change [3]. There is strong evidence that climate change impacts the amount, distribution and intensity of rainfall, which leads to more frequent droughts and floods in many parts of East African countries [4].

Meteorological drought is a natural hazard that severely disrupts the economy and agricultural activities. The research area would have been affected by drought, which resulted in reduced water harvesting activities, crop yields and damage to local food security. Erratic rainfall and its distribution are the main problems that affect the Wolaita Zone during agricultural operations. The amount of production and productivity are frequently impacted by erratic rainfall, which in turn has an impact on their means of livelihood [5]. In these cases, this research would have been analyzed to minimize the impacts of past and future projected meteorological drought effects in the study area. Since its invention, the global climate model's (GCM) output has been used in several studies to predict future rainfall changes in the Earth's climate [6]. The data were derived from the GCMs in the Coupled Model Intercomparison with Project Phase 6 (CMIP6) under Shared Socioeconomic Pathways (SSPs) via a statistical downscaling

technique [7]. This study compared the historical simulations of the CMIP6 models and analyze the projected meteorological drought may affect multiple perspectives [8].

Rainfall in the study area varies significantly in terms of amount, duration and distribution. The seasonal pattern of rainfall included Belg (February, March, April and May) rainfall; the amount received was considerably less than that received by Kiremt (June, July, August and September). In general, rainfall is bimodal in the study area [9]. The Wolaita Zone has a high population density and is highly dependent on labor-intensive and small-scale agriculture. According to the Wolaita Zone Finance and Economic Development Department (WZFEDD), rainfall in an area varies greatly in terms of its distribution and amount, typically decreasing from place to place [10]. In this area, earlier researchers have analyzed the effects of rainfall variability on household perceptions and its changes in the Wolaita Zone [11]. Nevertheless, the analysis of the variability of rainfall and characterization of (past and future projected) meteorological droughts has not been sufficiently investigated by other researchers. Therefore, this study analyzes and fills a gap in the literature by analyzing the variability of rainfall and characterizing (past and projected meteorological) drought over the Wolaita Zone, Ethiopia.

2. Materials and Methods

2.1. Description of the Study Area

Geographically, the Wolaita Zone is located between 6.4°-7.1° N and 37.4°-38.2° E. The Wolaita Zone is one of the zone administrations in Southern Ethiopia. The Wolaita Zone is located southwest of Addis Ababa, following the tarmac road from Shashemane to Arba Minch. Alternatively, it is located 330 km southwest of Addis Ababa, following the tarmac road that passes through Hosanna to Arba Minch. Sodo is established at the foot of Mount Damota and currently serves as the capital city of the Southern Ethiopian region and Wolaita Zone. Wolaita is bordered south by the Gamo Zone, west by the Omo River, which separates it from Dawro, northwest by the Kembata Zone and Tembaro Special Woreda, north by the Hadiya, northeast by the Oromia Region, east by the Bilate River, which separates it from the Sidama Region and southeast by Lake Abaya, which separates it from the Oromia Region, as shown in Figure 1.

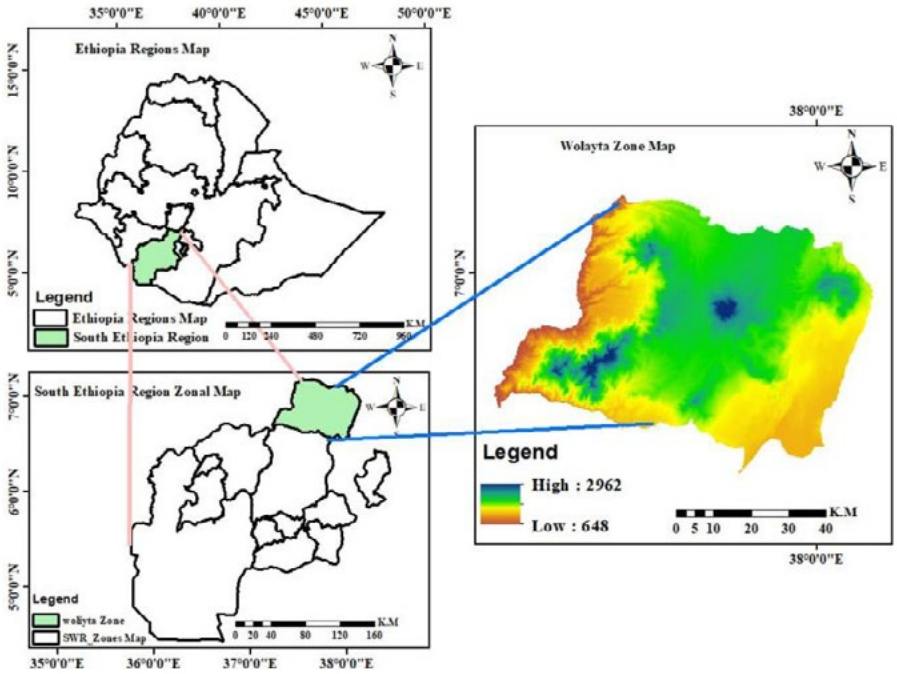

Figure 1: Study Area Map

There are approximately 1,527,908 people living in the Wolaita zone, with men making up 49.3% of the population and women making up 51.7% [12]. The altitude ranges from 501 meters at Bilate-Tena to 3000 meters above sea level at Damota Mountain. The mean annual rainfall in the Wolaita Zone varies from 817.5 mm at Bilate-Tena to 1500.33 mm at Mayokote. There are three agroecological zones in the study area: Kolla, Woyna-Dega and Dega. Each year, the average minimum and maximum temperatures are 15.5°C and 24.5°C, respectively. The rainfall distribution pattern is bimodal in the Wolaita Zone. The main rainy season, known as Kiremt, lasts from mid-June to the end of September. The Belg season, also known as the short (secondary) rainy season, lasts from mid-February to the end of May.

2.2 Data Types and Sources

2.2.1. Meteorological Data

The observed station data and grid data were collected from the Ethiopian Meteorology Institute (EMI). The stations for this study are selected on basis of their representativeness within a given agroecology and the length of the recording period. To cover the

study area, relatively long periods of rainfall data (1990–2020) with a reasonable geographical distribution from fifteen stations and daily gridded or Enhanced National Climate Services (ENACTS) rainfall data were used to fill in the missing data in this study. ENACTS is performed by improving the availability of timely, relevant and high-quality climate information at relevant spatiotemporal scales and working to promote the effective use of these data [13]. The following table shows the names of the stations used to perform the trend and variability of the rainfall analyses for this study.

No	Station Name	latitude	Longitude	Altitude
1	Abaya	6.62	37.83	1182 m
2	Areka	7.06	37.71	1752 m
3	Bedessa	6.87	37.94	1609 m
4	Bele	6.92	37.53	1240 m
5	Bilatetena	6.93	38.13	1496 m
6	Bilate	6.82	38.09	1361 m
7	Boditischool	6.96	37.86	2043 m
8	Bombe	7.14	37.58	1544 m
9	Danna1	6.63	37.57	1282 m
10	Gesuba	6.73	37.56	1522 m
11	Halale	6.75	37.34	1854 m
12	Humbotebela	6.70	37.77	1618 m
13	Mayokote	6.89	37.85	2121m
14	Shanto	7.03	37.86	1955 m
15	Wolaytasodo	6.82	37.75	1854 m

Table 1: Meteorological Stations Used for This Study Area

2.3. CMIP6 Climate Model Data

This study utilized global climate model (GCM) datasets from the CMIP6 models[14]. The CMIP6 model data were downloaded from the Earth System Grid Federation (ESGF) archives https://esgf-node.llnl.gov// search/cmip6. The definition of the SSP provides a new opportunity to examine the future in terms of physical climate change and global socioeconomic pathways. Furthermore, the datasets were grouped as baseline runs from 1985–2014 with two future time frames, referred to here after as mid-future (2041–2070) and far-future (2071–2100) [15]. The daily rainfall data under moderate (SSP2–4.5) scenarios and pessimistic or worst (SSP5–8.5) scenarios were used to estimate extreme rainfall events [15].

These SSP based scenarios consist of a set of baseline periods that describe future developments in the absence of climate change or new climate policies beyond those in place today, as well as mitigation scenarios that explore the implications of climate change mitigation policies applied to the baseline scenarios [16]. Compared with CMIP5 models, all CMIP6 models have more vertical layers and several advantages, including improved simulation accuracy in the stratosphere and a significant increase in the number of future scenarios investigated [17]. This study utilized the first realization (r1i1p1f1) of five models that have relatively high spatial resolutions (~1°). Table 2, presents the model description, including the spatial resolution, the institute(s) possessing intellectual property rights and the abbreviations of the dataset used. The study included a multimodel ensemble (MME) of the model datasets in its analyses.

Models	Institution	Resolution
BCC-CSM2-MR	Beijing Climate Center and China Meteorological Administration, China	1.13° × 1.13 °
CMCC-ESM2	Euro-Mediterranean Centre on Climate Change Coupled Climate Model	1.25°×0.94°
GFDL-ESM4	Geophysical Fluid Dynamics Laboratory (GFDL), USA	1.25° × 1.00°
MPI-ESM1-2-HR	Max Planck Institute, Germany	0.90° ×1.30°
MRI-ESM2-0	Meteorological Research Institute (MRI), Japan	1.13° × 1.13°

Table 2: Five Selected CMIP6 Climate Models for This Study

2.4. Data Quality Control

The data were checked for quality, recording length, missing data, and inhomogeneity. The missing data were obtained from the Enhanced National Climate Services (ENACTS) dataset. High-resolution satellite and station data were combined to fill in the gaps and record time inconsistencies in the observed rainfall data. This phenomenon is identified by the variations in the rainfall dataset, which could be caused by nonclimate factors such as instrumental inaccuracies, station relocations, and changes in instrumentation. Therefore, the homogeneity of the data series was checked via the standard normal homogeneity test [18]. The outliers of the data were checked and detected via Climate Data Tools (CDT).

2.5. Methods

2.5.1. Variability analysis

Coefficient of Variability (CV)

The coefficient of variation (CV) was used to analyze the annual, seasonal and monthly variabilities in rainfall via the following formula:

$$CV = \frac{\sigma}{X} * 100 \quad (1)$$

where: CV = coefficient variation, σ = standard deviation; and x = mean precipitation

The coefficient of variation was used to categorize the amount of rainfall variability [19].

Accordingly, CV < 20 = less variable; CV 20-30 = moderately variable; and CV >30 = highly variable.

Standardized Rainfall Anomaly (SRA)

The variability of rainfall was computed via the standardized rainfall anomaly (SRA) method [20]. The standardized rainfall anomaly (SRA) was calculated as the difference between the annual total of a particular year and the long-term average rainfall records divided by the standard deviation of the long-term data. This index is used to determine the interannual fluctuations of rainfall in the study area over the observation period and is represented mathematically as follows:

$$\mathrm{SRA} = \frac{\mathrm{Pt} - \mathrm{Pm}}{\sigma} \quad (2)$$

where: SRA is the standardized rainfall anomaly, Pt is the annual rainfall in year t, Pm is the long-term mean annual rainfall over the observation period, and σ is the standard deviation of the annual rainfall over the observation period. According to Harka et al., (2021), the Z values are classified as extremely wet (Z > 2), very wet (1.9 > Z > 1.5), moderately wet (1.49 > Z > 1.0), nearly normal (0.99 > Z > -0.99), moderately dry (-1.0 > Z > -1.49), severely dry (-1.5 > Z > -1.99), or extremely dry (Z < - 2) [21].

2.5.2. Trend Analysis

Modified Mann–Kendall Test: The Mann–Kendall (MK) statistic test is advised by the WMO for spotting trends in meteorological data [22,23,24]. This study applied the Mann–Kendall (MK) trend test method for historical and future rainfall data analysis via XLSTAT. A nonparametric technique called the Mann–Kendall (MK) test is used to identify trends in the time series of rainfall data. Therefore, before applying this test, we conducted the autocorrelation test suggested by [25]. For nonnormally distributed data series, such as rainfall data, the MK test is also recommended [26].

The monthly, seasonal and annual rainfall series were analyzed via the MK test. If the value in a time series is greater than its previous value, a score of +1 is given; conversely, a score of -1 is given. Let X1, X2, X3…….. X_n represent n data points, where X^j represents the data point at time j. Then, the Mann–Kendall statistics (S) are given by

$$S = \sum_{i=1}^{n-1} \sum_{j=i+1}^{n} Sign(Xj - Xi) \quad (3)$$

where the sign function is:

$$Sign(Xj - Xi) = \begin{cases} +1 \; Xj > Xi \\ 0 \; Xj = Xi \\ -1 \; Xj < Xi \end{cases} \quad (4)$$

where, X_j and X_i are the sequential data values in months j and i (j>i), respectively.

An increasing (upward) trend is shown by a positive value of S, whereas a decreasing (downward) trend is represented by a negative number. At the 0.01, 0.05, and 0.1 significance levels, the statistical significance of an increasing or decreasing trend in the mean precipitation and temperature values is assessed via a normalized test statistic (Z-score).

$$z = \begin{cases} \frac{S-1}{\sqrt{var(s)}} S > 0 \\ 0 \;\; S = 0 \\ \frac{S+1}{\sqrt{var(s)}} S < 0 \end{cases} \quad (5)$$

Where the variance of S is calculated as

$$Var(s) = \frac{1}{18}\left[n(n-1)(2n+5) - \sum_{i=1}^{g} ti(ti-1)(2ti+5)\right] \quad (6)$$

where, g is the number of tied groups, t_i is the number of tied values in the ith group, Var (S) is the reduction in the variance, and n is the number of data points.

This Z value and the Z value for (-1) from the standard normal distribution are compared to determine the significance.

Sen's Slope Estimator

Sen's slope estimator were used to determine the trend magnitude at a specific time [27,28]. Tests are frequently employed to measure the magnitude of trend in time series rainfall data [29,30]. The slope for all the data pairs can be calculated as follows:

$$Ti = \frac{Xj - Xi}{j - i} \; for \; i = 1,2,3, \ldots N \qquad (7)$$

where, Xj and Xi are the data values at times j and i (j>i), respectively. When there is one data point in each time period, $N = \frac{n(n-1)}{2}$, where n is the number of time periods. However, if there are more data points, then, $N < \frac{n(n-1)}{2}$, where n is the total number of observations. The values of N are arranged from smallest to largest. The median of these "n" values of Ti is then represented by Sen's slope of estimation, which is calculated via the following equation:

$$\begin{cases} \frac{T(N+1)}{2} \; for \; N \; odd \; observations \\ \frac{1}{2}\frac{(TN)}{2} + \frac{T(N+1)}{2} \; for \; N \; even \; observation \end{cases} \qquad (8)$$

A positive value of Q_i indicates an increasing magnitude, and a negative value of Q_i represents a decreasing magnitude.

2.5.3. Standard Precipitation Index (SPI)

The SPI was used for this investigation, which converts the rainfall parameter to a single numerical value to define the drought conditions of the study area [31]. The SPI allows for the determination of the duration, severity, and frequency of drought [32]. Its main advantage is that it is calculated for several time scales and identifies various drought types, such as meteorological, hydrological, and agricultural droughts [33]. Considering the minimum value of the SPI as the lower boundary and the maximum as the upper boundary of the uncertainty range, the uncertainty in the GCM projections was drawn for the period between 2041 and 2100 for SSP scenarios [34]. As a result, the SPI is calculated from the one-month rainfall data by first fitting the gamma probability distribution function and then transforming it into a normal distribution [31,35]. The alpha and beta parameters of the gamma probability density function are estimated for each station for different periods, including 1, 3, 6, 12, 24, and 48 months [36]. The gamma distribution is defined by its frequency or probability density function:

$$g(x) = \frac{1}{\beta^{\alpha}\Gamma(\alpha)} X^{\alpha-1} e^{\frac{-x}{\beta}} \; for \; x > 0 \qquad (9)$$

where; α > 0 is a shape parameter, β > 0 is a scale parameter, x is the rainfall amount and Γ (α) is the gamma function.

The parameters of the gamma probability density function may be estimated from the data sample via the maximum likelihood method for the station, for each time scale of interest, and for each month of the year.

Thus, we obtain:

$$\alpha = \frac{1}{4A}\left(1 + \sqrt{1 + \frac{4A}{3}}\right) \qquad (10)(a)$$

$$\beta = \frac{\overline{X}}{\alpha} \qquad (10)(b)$$

$$A = \ln(\overline{x}) - \frac{\sum \ln(x)}{n} \qquad (10)(c)$$

where, n = the number of precipitation observations

The resulting parameters are then used to find the cumulative probability of an observed precipitation event for the given month and time scale for the station in question. The cumulative probability is given by:

$$g(x) = \int_0^x g(x)d(x) = \frac{1}{\beta^{\alpha}\gamma(\alpha)} \int_0^x x^{\alpha-1} e^{\frac{-x}{\beta}} d(x) \qquad (11)$$

Lettingt = $\frac{\alpha}{\beta}$, this equation becomes the incomplete gamma function:

$$g(x) = \frac{1}{\gamma(\alpha)} \int_0^x t^{\alpha-1} e^{-t} \, d(t) \qquad (12)$$

Since g(x) is undefined for x=0 and a precipitation distribution may contain zeros, the cumulative probability becomes:

$$h(x) = q + (1 - q)g(x) \qquad (13)$$

where, q is the probability of zero and g(x) is the cumulative probability of the incomplete gamma function.

If m is the number of zeros in a precipitation time series, then q can be estimated by $\frac{m}{n}$. By applying Eq. (13), errors are eventually introduced to parameters α and β of the gamma distribution. These errors depend on the number of months with null precipitation (x = 0), and they are evident only for the 1-month precipitation. For longer time scales (e.g., 3 months, 6 months, etc.), the probability of precipitation was zero. This study evaluates the SPI index over one and three months. The cumulative probability, h(x), after its computation, is transformed to the standard normal random variable z with a mean equal to zero and a variance of one, which is the value of the SPI. The standard precipitation indices (SPI) and their interpretations are shown in Table 3

SPI Value	Drought Category
-2.00 and less	Extreme Drought
−1.50 to−1.99	Severe Drought
−1.00 to−1.49	Moderate Drought
0.99 to−0.99	Normal
1.00 to 1.49	Moderate Wet
1.50 to 1.99	Severe Wet
2.00 and more	Extreme Wet

Source: [30]

Table 3: SPI Values with Associated Drought Categories

Definitions of Drought Duration, Severity, Intensity and Frequency

To analyze the impact of drought events in the study area, the drought components of drought duration (DD), drought severity (DS), and drought frequency (DF) to detect the possible effects of drought events [37]. The study defines the DS and DF are defined as follows.

Drought durations (DD): The number of months between the start of a drought (included) and the end of a drought (not included) that determines the drought duration.

Drought severity (DS): The drought severity is the cumulative sum of the index values based on the duration extent.

$$S = \sum_{i=1}^{\text{Duration}} \text{Index} \qquad 14(a)$$

Drought intensity (DS): The intensity of a drought event is the severity divided by the duration of the event, as expressed in Eq. 14(b). Drought events that have a shorter duration and greater severity have greater intensities.

$$I = \frac{Severity}{Duration} \qquad 14(b)$$

Drought frequency (DF): The occurrence frequency is defined in Eq. 14(c) as follows:

$$F_s = \frac{n_s}{N_s} * 100 \qquad 14(c)$$

where ns is the number of drought events (SPI<−1.0), Ns is the total number of months for the study period, and s is a grid cell.

2.6. Model Performance Assessment Metrics

Differences in model data were quantified via three statistical metrics namely the correlation coefficient, mean error (ME), and relative bias (BIAS). The ME is a standard statistical metric used to measure model performance in fields such as meteorology and climate studies [38] the ME results are the average distance between simulated and observed values, and the metric does not indicate bias [39]. For ME, the lower the value is the better the fit, and 0 is the ideal result; ME ranges from -∞ to ∞. Relative bias (BIAS) measures systematic errors in calculating the differences between rainfall datasets [40].

$$\text{ME} = \frac{1}{n}\sum_{i=1}^{n}\left(X_i^{obs} - X_i^{sim}\right) \qquad 15$$

$$BIAS = \frac{\sum_{t=i}^{n}(X_i^{obs} - X_i^{sim})}{\sum_{t=1}^{n}(X_i^{obs})} \qquad 16$$

where, X_i^{sim} represents the simulated values of the ith day, X_i^{obs} represents the observed values of the ith day, P_i represents the precipitation values of the ith day, and n represents the number of points in the time series.

2.6.1. Climate Data Downscaling and Bias Correction

Before GCM outputs can be applied in real-world situations, they must be downscaled and bias corrected. This is mainly because the climate model outputs are biased due to imperfect conceptualization and parameterization, insufficient length of data records, quality of reference datasets and insufficient spatial resolution [41,42]. Therefore, this study uses the Climate Data Operator (CDO) to downscale the GCM climate models for the study periods from 2041–2070 and 2071–2100. GCM model output data often have a large bias, which requires correlation to monitor data bias reduction and increase data quality and reliability. It also serves as a channel to correlate GCM outputs to the climate model [4344,]. Before climate data are used for climate change impact studies and climate change assessment simulations, biases often need to be corrected [45]. Several bias correlation methods that outperform different methods under different conditions are available in the literature. In this study, I used the power transformation (PT) bias correction method to correct the statistical distribution function of the value simulated by the GCM relative to the distribution function of the observed data for rainfall. The power transformation (PT) method uses an exponential form to further adjust the standard deviation of the rainfall series. In this study, each monthly rainfall amount P_{raw} is transformed to a corrected rainfall amount P_{cor} via equation (17).

$$P_{cor} = \alpha * (P_{raw,mon})^b \qquad 17$$

The value of b was determined such that the CV of the corrected monthly (mon) rainfall matched that of the monthly (mon)

observed rainfall. The parameter α was then determined such that the mean of the corrected monthly rainfall value corresponded with the observed mean monthly rainfall. These data were added to the CMhyd platform to perform bias correction. The CMhyd selects the closest observed station to the climate model grid cells to compare the observed and simulated time series, i.e., those considered in the bias correction process [46].

3. Results and Discussion

3.1. Variability and Trends of Rainfall

3.1.1. Variability of Rainfall

The mean annual and seasonal rainfall variabilities in the Wolaita Zone are presented in Table 4. The research area experiences bimodal rainfall and receives high amounts of rainfall during the Kiremt season, which is the main rainy season. The Belg rainfall contributes a small amount of the total rainfall. The mean annual rainfall in the study area was 1149.61 mm. However, the seasonal rainfall variability was highest from February to May in the Belg season and lowest in the Kiremt season from June to August in the Wolaita Zone. The Belg rainfall is much more variable than the summer (Kiremt) rainfall distribution variation. The Kiremt rainfall distribution is more variable than the annual rainfall distribution variation across the study area.

	Annual		Belg		Kiremt	
Stations	**Mean**	**CV (%)**	**Mean**	**CV (%)**	**Mean**	**CV (%)**
Abaya	766.53	22.77	306.41	32.88	309.76	37.08
Areka	1377.02	27.12	475.07	36.55	700.44	32.66
Bedessa	1049.58	24.42	357.43	41.73	545.67	30.20
Bele	1208.08	53.88	352.24	34.15	586.35	40.49
Bilatetena	921.29	30.65	351.31	35.98	368.42	41.18
Bilate	817.51	23.84	315.66	38.79	315.99	29.80
Boditischool	1224.33	15.82	470.44	30.21	558.05	22.68
Bombe	1374.79	29.65	497.39	33.64	687.03	40.87
Danna1	1200.13	25.12	430.18	37.09	560.59	35.87
Gesuba	1007.49	27.11	398.10	31.34	429.67	36.62
Halale	1230.21	27.48	465.17	30.62	551.26	41.88
Humbotebela	1110.59	24.22	375.37	28.68	530.64	40.70
Mayokote	1500.33	28.06	558.25	48.81	687.26	45.64
Shanto	1124.24	16.59	426.53	33.26	531.82	23.10
Wolaita sodo	1332.08	16.92	472.77	28.51	635.91	25.13

Table 4: Mean (Annual and Seasonal) Rainfall and Coefficient of Variation From 1990–2020

3.1.2. Standardized Rainfall Anomaly Index

The standard rainfall anomalies were computed, and the results indicate that there were positive and negative anomalies, which implies the presence of annual and seasonal rainfall variability across the observed time series in the study area. For the annual standardized rainfall, the highest positive anomaly (+2.13) was observed in 2020, and the lowest negative anomaly (−1.61) was observed in 1990. The annual negative anomaly exceeded the positive anomaly in all years; there was also high variability; a dry year was followed by another two or three dry years and then replaced by wet years across the study area. Because of the rainfall variability over the study area, the highest values represent the highest rainfall recorded, and the lowest values also represent the lowest rainfall recorded. Generally, a positive value in the figure below indicates wet year anomalies, and a negative value indicates dry anomalies of the rainfall variability in the study area.

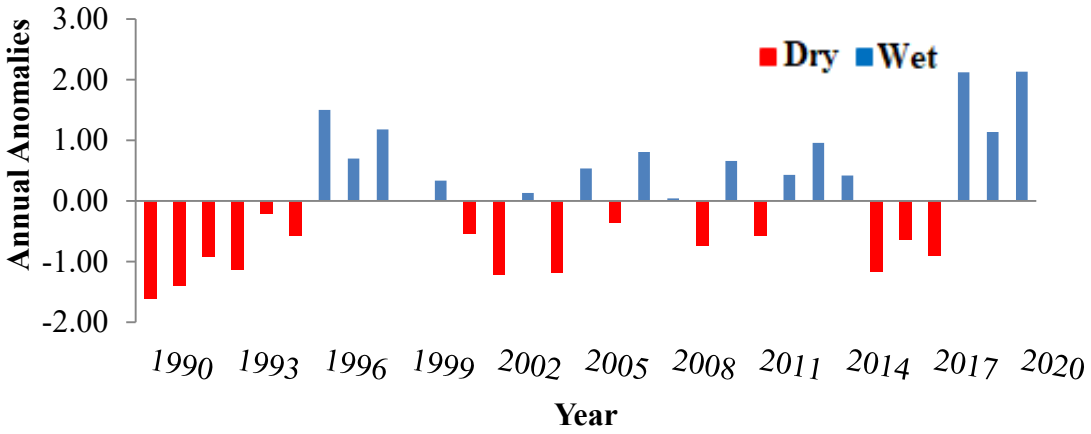

Figure 2: Standardized Annual Rainfall Anomalies

3.1.3. Trends of Rainfall

The Kiremt and annual rainfall data indicate a declining trend at three and two stations, respectively, even though the Kiremt rainfall data are not statistically significant except at the Halale and Shanto stations, where there is a statistically significant ($P < 0.05$) reduction in the Kiremt rainfall trend, as shown in Table 5. However, Bilatetena, Halale, and Shanto registered significant increases in the annual rainfall of the Wolaita Zone. The Belg season rainfall shows no statistically significant increasing trend ($P < 0.05$) at any of the 15 stations. Generally, the direction and magnitude of the seasonal rainfall trend were not uniform across the different stations.

	Annual			Belg-season			Kiremt-season		
Stations	**Z**	**Q**	**P_value**	**Z**	**Q**	**P_value**	**Z**	**Q**	**P_value**
Abaya	0.19	8.24	0.14	-0.02	-0.38	0.92	0.20	5.47	0.11
Areka	0.03	0.40	0.80	-0.13	-2.67	0.32	0.18	3.56	0.16
Bedessa	-0.05	-2.59	0.74	-0.07	-2.06	0.61	-0.05	-1.50	0.69
Bele	-0.02	-1.66	0.87	-0.07	-1.09	0.59	0.08	2.26	0.54
Bilatetena	0.35	11.20	0.00	0.07	1.47	0.57	0.23	5.84	0.08
Bilate	0.14	6.47	0.30	0.15	2.32	0.25	0.14	3.17	0.27
Bodity	-0.23	-12.56	0.07	-0.23	-5.88	0.07	0.25	9.91	0.05
Bombe	0.23	15.51	0.07	0.03	0.50	0.80	-0.06	9.91	0.66
Danna1	-0.02	-0.63	0.87	-0.08	-1.11	0.57	0.08	2.85	0.54
Gesuba	0.16	5.43	0.21	0.02	0.55	0.87	0.23	3.19	0.07
Halale	0.28	8.76	0.03	0.06	1.48	0.64	0.26	4.20	0.04
Humbotebela	0.20	6.95	0.13	-0.18	-2.82	0.17	0.18	6.59	0.15
Mayokote	0.02	0.50	0.91	-0.13	-3.25	0.31	0.10	2.57	0.46
Shanto	0.39	21.25	0.00	0.01	0.44	0.97	0.47	16.95	0.00
Wolaita sodo	0.14	4.54	0.26	0.06	1.14	0.67	0.10	2.02	0.46

Bold values indicate a significance level of $P < 0.05$.

Table 5: Mann–Kendall (Z) and Sen's slope (Q) Trend Test (mm/year) Results for the Annual, Belg, and Kiremt Rainfall at the Selected Stations in the Wolaita Zone, Southern Ethiopia

3.1.4. Monthly Rainfall Variability

The mean monthly rainfall distribution in the Wolaita Zone varied from 25.22 to 150.11 mm from 1990–2020 (Figure 3). Comparatively, the monthly rainfall was low in December, January, and February. Moreover, relatively intensive rainfall was recorded as 190.65 mm in May and 206.68 mm in August. The monthly rainfall peaks in April (188.68 mm), May (190.65 mm), July (206.45 mm) and August (206.68 mm). The minimum monthly rainfall was recorded in December (14.14 mm) and January (11.39 mm). Generally, the maximum value represents the sum of the highest rainfall recorded per month, the minimum value represents the sum of the minimum or lowest rainfall recorded per month, and the mean values represent the average of the highest and the lowest rainfall recorded per month over the study area.

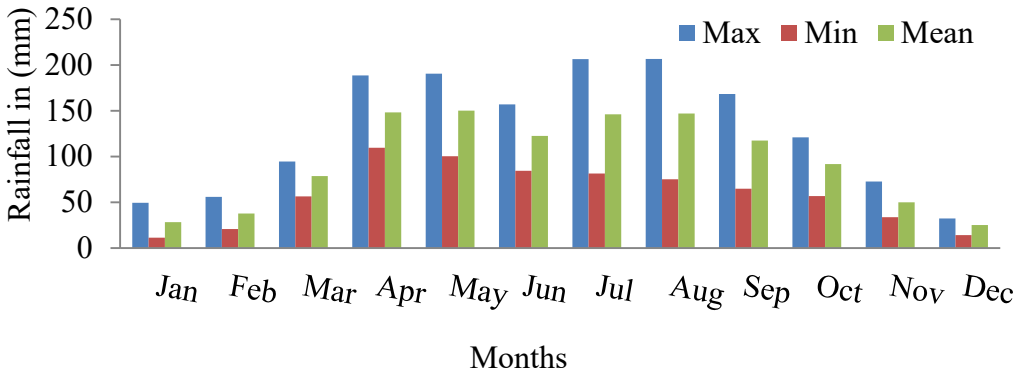

Figure 3: Maximum, Minimum, and Mean Monthly Rainfall Distributions

3.1.5. Annual and Seasonal Rainfall Trends

Figure 4 shows the annual and seasonal rainfall over the Wolaita Zone. From 1990–2020, the annual rainfall ranged from 910.3 mm to 1465.9 mm. The highest annual rainfall, 1465.9 mm, was recorded in 2020. The minimum annual rainfall, 910.3 mm, was recorded in 1990. In the Belg season, the highest rainfall, 694.5 mm, was recorded in 2018. The minimum value which was 309.3 mm, recorded in the 2019. In the Kiremt season, the highest rainfall, 752.8 mm recorded in 2019. The minimum value was 379.5 mm, recorded in 1990. The variability in the annual and seasonal rainfall represented similar increases in amount and distribution, except for a few years when an extremely high rainfall distribution was recorded over the study area. Generally, when there is variability in the rainfall distribution across the research area, some years usually have the highest and some years have the lowest rainfall distributions recorded over the study area.

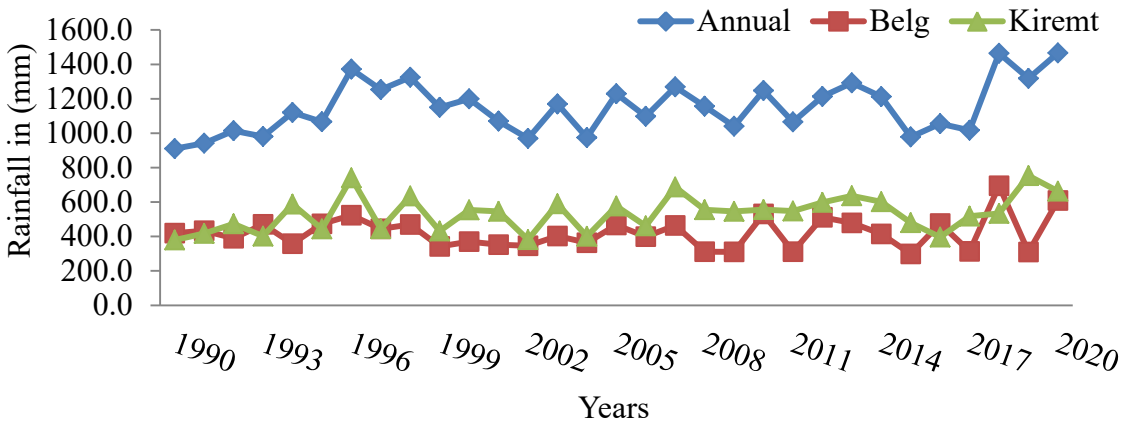

Figure 4: Annual and Seasonal Rainfall Distribution Variation From 1990–2020

3.1.6. Spatial Distribution of Mean Seasonal and Mean Annual Rainfall

Figure 5 shows the spatial distribution of the seasonal and annual rainfall in the Wolaita Zone. In the Belg season, the southeastern parts of the Wolaita Zone are dominated by decreasing rainfall. However, significant decreasing and increasing rainfall trends occurred in the southwestern, western, and northeastern parts of the Wolaita Zone. The remaining part of the Wolaita Zone is dominated by an increasing rainfall distribution. The spatial distribution of Belg rainfall shows that the rainfall of the eastern, southern, and southeastern parts of the Wolaita Zone is less than the average rainfall value, whereas the northern, western, central, and southwestern parts of the Wolaita Zone receive more rainfall than the average.

The rainfall in the Kiremt season represents dominance-increasing distribution in most parts of the Wolaita Zone. In general, some parts of the southern, southwestern, southeastern, central, and northeastern parts of the Wolaita Zone represent significantly decreasing rainfall distributions, whereas the northern, northwestern, and central parts of the Wolaita Zone represent significantly increasing rainfall distributions.

The spatial distribution pattern of annual rainfall reflects the combined effect of seasonal rainfall. The rainfall distribution decreases in the southern, southwestern, southeastern, and eastern parts of the Wolaita Zone. The remaining parts of the Wolaita Zone show increasing rainfall distributions. The rainfall distribution map of the Wolaita Zone revealed that the annual rainfall value ranged from 910.3 mm to 1465.9 mm.

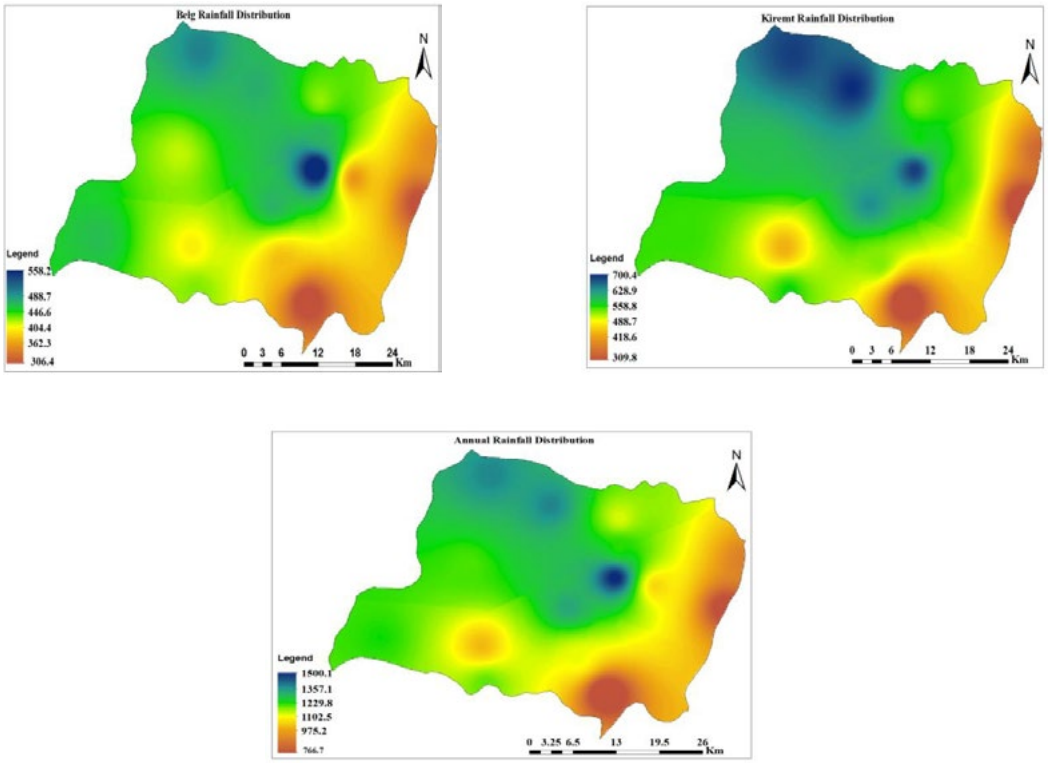

Figure 5: Spatial Distribution of Annual and Seasonal Rainfall

3.2. Bias Correction of the CMIP6 Model Simulations

The model's capacity for ensemble mean values and observed values is used to determine the accuracy of future projected changes over the study area [47,48]. After bias correction, the three selected models show the best performance. These selected models are the Beijing Climate Center (BCC) and China Meteorological Administration (CMA), China (BCC-CSM2-MR) Model; Geophysical Fluid Dynamics Laboratory, USA (GFDL-ESM4) Model, and Meteorological Research Institute (MRI), Japan (MRI-ESM2-0) Model. According to Ayugi et al., (2022) in this study the best-performing selected GCM models are based on previous studies [37]. The present results agree with existing findings and support corrections for GCM biases before employing data for impact research [47,49,50].

The ensemble means were combined with multiple other models in the study period. Compared with the other individual GCMs, the ensemble means of the GCMs performed better in terms of the correlation metric and had a greater correlation with the observed rainfall [51]. As a result, understanding the contributions of GCMs uncertainty is critical for analyzing drought in this study area.

GCM models	CORR	ME (mm)	BIAS (%)
BCC-CSM2-MR	0.7	7.4	1.1
GFDL-ESM4	0.7	3.4	1.0
MRI-ESM2-0	0.6	2.1	1.0
Ensemble	0.8	2.0	1.0

Table 6: GCM Model Performance Assessment and Statistical Metric Criteria

3.2.1. Simulated CMIP6 Models and Observed Rainfall

The GCMs model rainfall was overestimated and underestimated compared with the ensemble mean and observed rainfall in the study area. The ensemble mean and observed rainfall data compared with other individual GCM model rainfall data outputs are illustrated in Figure 8. The BCC-CSM2-MR and GFDL-ESM4 models overestimated the mean and observed rainfall compared with the ensemble model. Compared with ensemble model mean and observed rainfall the MRI-ESM2-0 model is underestimated. The results indicate that the simulated ensemble mean rainfall data are close to the observed rainfall data.

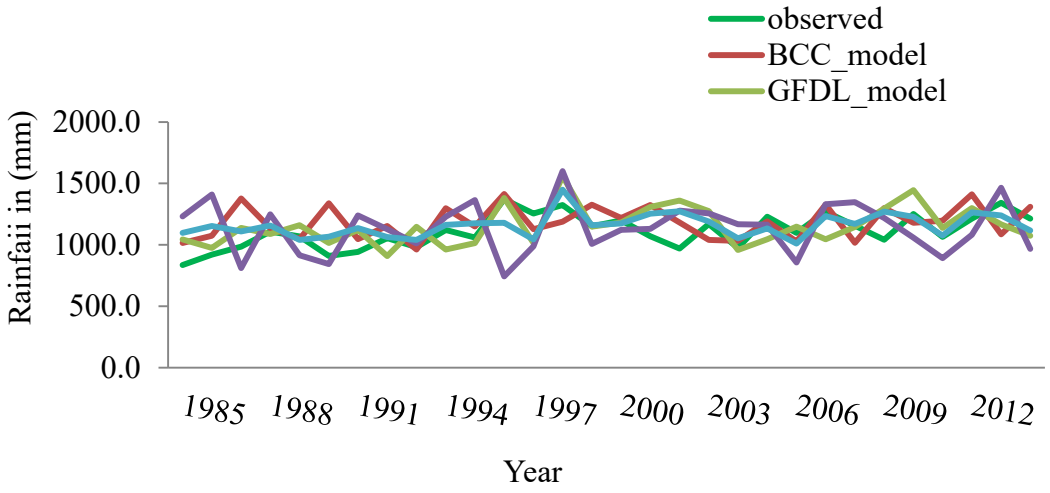

Figure 6: Observed Rainfall and GCM Simulated Baseline Rainfall From 1985–2014

3.2.2. Historical Meteorological Drought Events

To assess the ability of the CMIP6 model to predict meteorological drought effects across the Wolaita Zone. The SPI was first calculated via observed and bias-corrected GCM model rainfall and then calculated after drought events. The observed and ensemble means of the SPI (30 and 90) days were analyzed to show that meteorological drought events were recorded from 1985–2014. The study area drought index indicated that the multimodel ensemble means frequent drought and normal conditions or drought at different time scales (30 and 90 days) across the study area.

Compared with each other, multimodel ensemble means and observation periods have effects on the meteorological drought, and the drought pattern and frequencies are similar at both time periods. The SPI is the drought index, which indicates drought conditions at different severity levels that range from no drought to extreme drought conditions. In the multimodel ensemble mean, moderate drought was more frequent than it was during the multimodel observation period. Extreme droughts in 1987 and 2005 (SPI-30 and SPI-90) occurred at the left panels. Severe droughts occurred on both the right and left panels of the Wolaita Zone in 1986, 1987, 1990, 2004, 2008, and 2012 (SPI-30 and SPI-90). Moderate droughts occurred during the both right and left panels in 1989, 1994, and 2008 (SPI-30 and SPI-90), as shown in Fig. 7 (left panels).

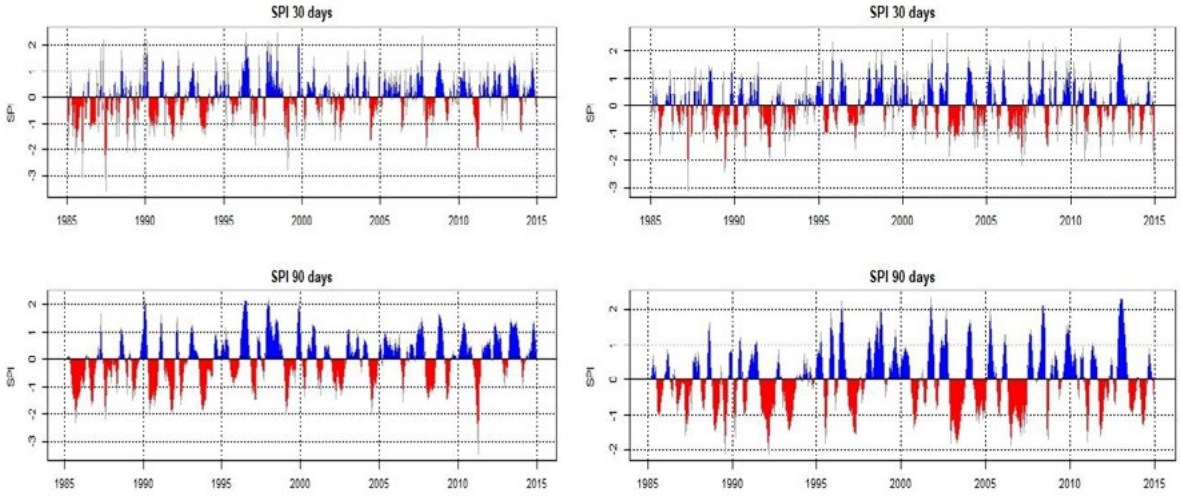

Figure 7: Observed (left panel) and Multimodel Ensemble Mean (Right Panel) Meteorological Drought From 1985–2014

3.2.3. Historical Trends in Meteorological Drought Events

Initially, the MK test is performed to check the significance of a trend. The bold values in the table indicate significant values. The Mann–Kendall trend test was conducted to determine whether the trend increased or decreased across the different time series in the study area. The results of the Mann–Kendall trend test for the observed and ensemble mean periods indicate an increasing trend or upward trends at the SPI-30 and SPI-90 days at the 95% confidence level. The results indicate that the area in the models' ensemble mean trends is insignificant for the SPI-30 and SPI-90 days, but the trends are significant for the SPI-30 and SPI-90 days at the observed times, as shown in Table 7.

Days	Observed			Ensemble Mean		
	Tau	Sen's slope	P–value	Tau	Sen's slope	P–value
30	0.119	0.002	**0.001**	0.058	0.001	0.101
90	0.172	0.003	**0.000**	0.083	0.001	0.019

Bold values indicate statistically significant trends.

Table 7: Mann–Kendal (Tau) Statistics and Sen's Slope Trend Test Results for the Observed and Ensemble Mean Periods of Meteorological Drought with a Significance Level of P < 0.05

3.2.4. Future Projected Changes in Meteorological Drought Events

Figure 8 (left and right panels) depicts the multimodel ensemble mean increases in drought duration in the middle future (2041–2070) and far future (2071–2100) for various emission scenarios based on the baseline period from 1985–2014. The projected changes in drought frequency are greater in the far future (2071–2100) under the SSP2–4.5 and SSP5–8.5 scenarios than in the middle future (2041–2070) under the SSP2–4.5 and SSP5–8.5 scenarios of the projection of future changes in drought intensity in the Wolaita Zone.

Projected future meteorological droughts will increase in the study areas from 2041–2070 under the SSP2–4.5 scenario but decrease in intensity in the study areas from 2071–2100 under the SSP5–8.5 scenario. The drought intensity is projected to follow a diverse pattern of drought changes under different emission scenarios. The analysis of the SPI with varying time scales was derived from three bias-corrected GCM models over the Wolaita Zone. For SPI-30 and SPI-90 days, extreme droughts are expected in 2044, 2046, and 2063 under the SSP2–4.5 and SSP5–8.5 scenarios in the mid-future. Severe droughts are expected in 2044, 2046, 2052, 2056, 2062, 2068, and 2070 under the SSP2–4.5 and SSP5–8.5 scenarios in the mid-future, and moderate droughts are expected in 2041, 2043, 2058, 2066, and 2068 under the SSP2–4.5 and SSP5–8.5 scenarios relative to the baseline period of the study area. At the (SPI-30 and SPI-90) days, extreme droughts will be expected in the years 2073, 2075, and 2086 under the SSP2–4.5 and SSP5–8.5 scenarios in the far-future. Severe droughts are expected in 2073, 2076, 2079, 2083, 2093, and 2100, and moderate droughts are expected in 2071, 2077, 2079, 2083, and 2097 under the SSP2–4.5 and SSP5–8.5 scenarios in the far-future relative to the baseline period of the study area. The results of the study area will experience a similar number of frequent droughts in the mid-future (2041–2070) under SSP2–4.5 and SSP5–8.5 compared with the far-future (2071–2100) under the SSP2–4.5 and SSP5–8.5 scenarios. Meteorological droughts in the far-future under the two scenarios are more frequent and intense than that in the mid-future under the two scenarios. In general, the meteorological drought severity and frequency in the middle and far-future under the SSP2–4.5 and SSP5–8.5 scenarios from 2041–2100 are more frequent and intense than those in the base period from 1985–2014.

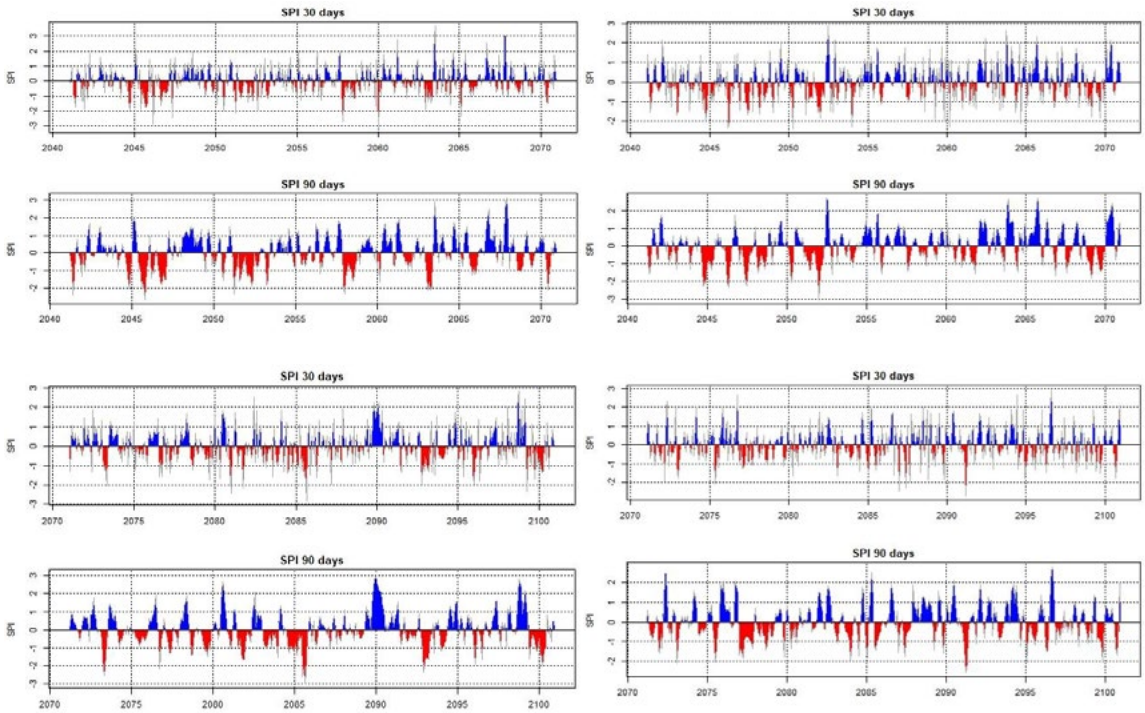

Figure 8: Projected Changes in the Drought (Top Right and Left Panels) in the Near Future (2041–2070) Under SSP2–4.5 and SSP5–8.5 Scenarios and (Bottom right and left panels) in the Far Future (2071–2100) Under SSP2–4.5 and SSP5–8.5 Scenarios

3.2.5. Future Trend Changes in Drought

Initially, the MK test is performed to check the significance of a trend. The bold values in the table indicate significant values. A statistical test was conducted to check whether a trend existed in the SPI at different time series in the study area via the Mann–Kendall. The Mann–Kendall trend test in the mid-future (2041–2070) under the SSP2–4.5 and SSP5–8.5 scenarios revealed increasing trends in the SPI values on SPI-30 and SPI-90 days at the 95% confidence level. A negative trend was observed in the far-future (2071–2100) under the SSP2–4.5 and SSP5–8.5 scenarios; however, the trend was statistically insignificant in the middle and far-future at all SPI time scales except in the far-future (2071–2100) under the SSP2–4.5 scenarios at the (SPI-90) days at the 95% confidence level. The results in the Table 8 blow indicate that the areas in the middle and far-future trends are insignificant under both the SSP2–4.5 and SSP5–8.5 scenarios. In general, during the historical period, a positive trend was observed on the SPI-30 and SPI-90 days compared with the future projected periods under the SSP2–4.5 and SSP5–8.5 scenarios. The mid-future trend will show a positive trend under the SSP2–4.5 and SSP5–8.5 scenarios on SPI-30 and SPI-90 days, but there will be a negative trend in the far-future under the SSP2–4.5 and SSP5–8.5 scenarios on SPI-30 and SPI-90 days. A summary of the MK test results in the middle and far future periods is presented in Table 8.

Day	SSP2–4.5 (2041–2070)			SSP2–4.5 (2071–2100)			SSP5–8.5 (2041–2070)			SSP5–8.5 (2071–2100)		
	Tau	Sen's slope	P–value	Tau	Sen's slope	P–value	Tau	Sen's slope	P–value	Tau	Sen's slope	P–value
30	0.021	0.000	0.528	-0.094	-0.001	0.008	0.006	0.00	0.874	-0.011	0.000	0.760
90	0.010	0.000	0.865	-0.108	-0.002	0.002	0.040	0.001	0.257	-0.053	-0.001	0.133

Bold values indicate statistically significant trends, whereas unbold values indicate statistically insignificant trends.

Table 8: Mann–Kendal (Tau) Statistics and Sen's Slope Trend Test Results for Two Different Future Scenarios of Drought with A Significance Level of P < 0.05

4. Conclusions

This research aims to determine the variability in rainfall at the observed time from 1990–2020 over the Wolaita Zone. Additionally, the duration, frequency, and severity of the (past and future projected) meteorological drought with a base period from 1985–2014 and a future projection from 2041–2100 were used for this study. The spring (belg) rainfall is much more variable than the summer (Kiremt) and annual rainfall. Spatial and temporal variations in rainfall have been determined at mean monthly, seasonal, and annual time scales. The modified Mann–Kendall test was used to determine the upward or downward trend, and Sen's slope estimator was used to determine the magnitude of increase or decrease. The Kiremt rainfall data indicate a decreasing trend at two and three stations, although the Kiremt rainfall data are insignificant except at the Halale and Shanto stations, which are statistically significant at $P < 0.05$. The historical period, shows a positive or upward trend at the SPI-30 and SPI-90 days compared with the mid-future period, which show a positive or upward trend under the SSP2–4.5 and SSP5–8.5 scenarios at the SPI-30 and SPI-90 days but the far-future period, shows a negative or downward trend under the SSP2–4.5 and SSP5–8.5 scenarios at the SPI-30 and SPI-90 days, which are statistically significant at $P < 0.05$.

Additionally, this study employed bias-corrected CMIP6 (GCM) data to assess the historical and future changes in meteorological drought over the Wolaita Zone. Two scenarios (SSP2–4.5 and SSP5–8.5) were used to determine future projected changes in meteorological drought at two time scales during the mid-future (2041–2070) and far-future (2071–2100) relative to a baseline period (1985–2014). In the far-future (2070–2100), under the SSP2–4.5 and SSP5–8.5 scenarios, meteorological drought will be more frequent and intense than in the mid-future (2041–2070) under the SSP2–4.5 and SSP5–8.5 scenarios. Future projected meteorological drought in the study area will be more affected by extreme, severe, and moderate drought during the middle and far-future under the SSP2–4.5 and SSP5–8.5 scenarios, which is more frequent and intense than the historical period over the study area. However, current SPI prescriptions cannot be used to accurately determine the exact times of drought periods or monitor meteorological droughts below the one-month scale.

References

1. Weldegerima, T. M., Zeleke, T. T., Birhanu, B. S., Zaitchik, B. F., & Fetene, Z. A. (2018). Analysis of rainfall trends and its relationship with SST signals in the Lake Tana Basin, Ethiopia. *Advances in Meteorology, 2018*(1), 5869010.
2. Indeje, M., Semazzi, F. H., & Ogallo, L. J. (2000). ENSO signals in East African rainfall seasons. *International Journal of Climatology: A Journal of the Royal Meteorological Society, 20*(1), 19-46.
3. Rahmani, V., & Harrington Jr, J. (2019). Assessment of climate change for extreme precipitation indices: A case study from the central United States. *International Journal of Climatology, 39*(2), 1013-1025.
4. Gyamfi, C., Amaning-Adjei, K., Anornu, G. K., Ndambuki, J. M., & Odai, S. N. (2019). Evolutional characteristics of hydro-meteorological drought studied using standardized indices and wavelet analysis. *Modeling Earth Systems and Environment, 5*, 455-469.
5. Ladejinsky, W. (1976). Agricultural production and constraints.
6. Girma, R., Fürst, C., & Moges, A. (2022). Performance evaluation of CORDEX-Africa regional climate models in simulating climate variables over Ethiopian main rift valley: evidence from Gidabo river basin for impact modeling studies. *Dynamics of Atmospheres and Oceans, 99*, 101317.

7. Hamlet, A. F., Salathé, E. P., & Carrasco, P. (2010). Statistical downscaling techniques for global climate model simulations of temperature and precipitation with application to water resources planning studies.
8. Rettie, F. M., Gayler, S., Weber, T. K., Tesfaye, K., & Streck, T. (2023). Comprehensive assessment of climate extremes in high-resolution CMIP6 projections for Ethiopia. *Frontiers in Environmental Science, 11,* 1127265.
9. Gebremichael, A., Quraishi, S., & Mamo, G. (2014). Analysis of seasonal rainfall variability for agricultural water resource management in southern region, Ethiopia. *Journal of Natural Sciences Research, 4*(11), 56-79.
10. Finance, W. Z. (2007). Economic Development Department (2017). *Wolaita Zone Finance and Economic Development Department Data Collection, Organization and Dissemination Work Process Annual Abstract, Wolaita Soddo, SNNPRS, Ethiopia.*
11. Esayas, B., Simane, B., Teferi, E., Ongoma, V., & Tefera, N. (2019). Climate variability and farmers' perception in Southern Ethiopia. *Advances in Meteorology, 2019*(1), 7341465.
12. Gizaw, W., & Assegid, D. (2021). Trend of cereal crops production area and productivity, in Ethiopia. *Journal of Cereals and Oilseeds, 12*(1), 9-17.
13. Dinku, T., Thomson, M. C., Cousin, R., del Corral, J., Ceccato, P., Hansen, J., & Connor, S. J. (2018). Enhancing national climate services (ENACTS) for development in Africa. *Climate and Development, 10*(7), 664-672.
14. Mitchell, D. (2017). Interactive comment on "Half a degree Additional warming, Projections, Prognosis and Impacts (HAPPI): Background and Experimental Design" by Daniel Mitchell et al. Geosci. *Model Dev. Discuss, 10*, 571-583.
15. Ayugi, B., Dike, V., Ngoma, H., Babaousmail, H., Mumo, R., & Ongoma, V. (2021). Future changes in precipitation extremes over East Africa based on CMIP6 models. *Water, 13*(17), 2358.
16. O'Neill, B. C., Kriegler, E., Ebi, K. L., Kemp-Benedict, E., Riahi, K., Rothman, D. S., ... & Solecki, W. (2017). The roads ahead: Narratives for shared socioeconomic pathways describing world futures in the 21st century. *Global environmental change, 42,* 169-180.
17. Gupta, V., Singh, V., & Jain, M. K. (2020). Assessment of precipitation extremes in India during the 21st century under SSP1-1.9 mitigation scenarios of CMIP6 GCMs. *Journal of Hydrology, 590*, 125422.
18. Manatsa, D., Chingombe, W., & Matarira, C. H. (2008). The impact of the positive Indian Ocean dipole on Zimbabwe droughts. *International Journal of Climatology, 28*(15), 2011.
19. Nicholson, S. E. (1985). Sub-saharan rainfall 1981–84. *Journal of climate and applied meteorology, 24*(12), 1388-1391.
20. Agnew, C. T., & Chappell, A. (1999). Drought in the Sahel. *GeoJournal, 48,* 299-311.
21. Harka, A. E., Jilo, N. B., & Behulu, F. (2021). Spatial-temporal rainfall trend and variability assessment in the Upper Wabe Shebelle River Basin, Ethiopia: Application of innovative trend analysis method. *Journal of Hydrology: Regional Studies, 37,* 100915.
22. Gautam, M., & Singh, A. K. (2015). Impact of climate change on water resources. *Climate Change Modelling, Planning and Policy for Agriculture,* 219-231.
23. Mann, H. B. (1945). Nonparametric tests against trend. *Econometrica: Journal of the econometric society,* 245-259.
24. WMO, W. (1988). Analyzinglong time series of hydrological data with respectto climate variability. *Geneva: WMO secretariat.*
25. Alexander, L. V., Tapper, N., Zhang, X., Fowler, H. J., Tebaldi, C., & Lynch, A. (2009). Climate extremes: progress and future directions. *International Journal of Climatology: A Journal of the Royal Meteorological Society, 29*(3), 317-319.
26. Moshinsky, M. (1959). Transformation brackets for harmonic oscillator functions. *Nuclear Physics, 13*(1), 104-116.
27. Sen, P. K. (1968). Estimates of the regression coefficient based on Kendall's tau. *Journal of the American statistical association, 63*(324), 1379-1389.
28. Theil, H. (1950). A rank-invariant method of linear and polynomial regression analysis. *Indagationes mathematicae, 12*(85), 173.
29. Jain, S. K., & Kumar, V. (2012). Trend analysis of rainfall and temperature data for India. *Current Science,* 37-49.
30. Mondal, A., Kundu, S., & Mukhopadhyay, A. (2012). Rainfall trend analysis by Mann-Kendall test: A case study of north-eastern part of Cuttack district, Orissa. *International Journal of Geology, Earth and Environmental Sciences, 2*(1), 70-78.
31. Iwata, T., Nishiyama, N., Nagano, K., Izumi, N., Tsukioka, T., Chung, K., ... & Suehiro, S. (2012). Preoperative serum value of sialyl Lewis X predicts pathological nodal extension and survival in patients with surgically treated small cell lung cancer. *Journal of surgical oncology, 105*(8), 818-824.
32. Hayes, M. J., Svoboda, M. D., Wiihite, D. A., & Vanyarkho, O. V. (1999). Monitoring the 1996 drought using the standardized precipitation index. *Bulletin of the American meteorological society, 80*(3), 429-438.
33. McKee, T. B., Doesken, N. J., & Kleist, J. (1995, January). Drought monitoring with multiple time scales. PROCEEDINGS OF THE CONFERENCE ON APPLIED CLIMATOLOGY.
34. Haile, G. G., Tang, Q., Hosseini-Moghari, S. M., Liu, X., Gebremicael, T. G., Leng, G., ... & Yun, X. (2020). Projected impacts of climate change on drought patterns over East Africa. *Earth's Future, 8*(7), e2020EF001502.
35. Edwards, D. C., & McKee, T. B. (1997). Characteristics of 20th century drought in the United States at multiple time scales.
36. Svoboda, M., Hayes, M., & Wood, D. (2012). Standardized precipitation index: user guide.
37. Ayugi, B., Shilenje, Z. W., Babaousmail, H., Lim Kam Sian, K. T., Mumo, R., Dike, V. N., ... & Ongoma, V. (2022). Projected changes in meteorological drought over East Africa inferred from bias-adjusted CMIP6 models. *Natural Hazards, 113*(2), 1151-1176.
38. Hodson, T. O. (2022). Root mean square error (RMSE) or mean absolute error (MAE): When to use them or not.

Geoscientific Model Development Discussions, 2022, 1-10.
39. Jackson, E. K., Roberts, W., Nelsen, B., Williams, G. P., Nelson, E. J., & Ames, D. P. (2019). Introductory overview: Error metrics for hydrologic modelling–A review of common practices and an open source library to facilitate use and adoption. *Environmental Modelling & Software, 119*, 32-48.
40. Meng, J., Li, L., Hao, Z., Wang, J., & Shao, Q. (2014). Suitability of TRMM satellite rainfall in driving a distributed hydrological model in the source region of Yellow River. *Journal of Hydrology, 509,* 320-332.
41. Gudmundsson, L., Bremnes, J. B., Haugen, J. E., & Engen-Skaugen, T. (2012). Downscaling RCM precipitation to the station scale using statistical transformations–a comparison of methods. *Hydrology and Earth System Sciences, 16*(9), 3383-3390.
42. Sarvina, Y., Pluntke, T., & Bernhofer, C. (2019). Comparing bias correction methods to improve modelled precipitation extremes. *Jurnal Meteorologi dan Geofisika, 19*(2), 103-110.
43. Hawkins, E., Osborne, T. M., Ho, C. K., & Challinor, A. J. (2013). Calibration and bias correction of climate projections for crop modelling: An idealised case study over Europe. *Agricultural and forest meteorology, 170*, 19-31.
44. Gebrechorkos, S. H., Hülsmann, S., & Bernhofer, C. (2019). Statistically downscaled climate dataset for East Africa. *Scientific data, 6*(1), 31.
45. Christensen, J. H., Hewitson, B., Busuioc, A., Chen, A., Gao, X., Held, I., ... & Whetton, P. (2007). *Regional climate projections*. Chapter 11.
46. Brighenti, T. M., Gassman, P. W., Gutowski Jr, W. J., & Thompson, J. R. (2023). Assessing the influence of a bias correction method on future climate scenarios using SWAT as an impact model indicator. *Water, 15*(4), 750.
47. Piani, C., Haerter, J. O., & Coppola, E. (2010). Statistical bias correction for daily precipitation in regional climate models over Europe. *Theoretical and applied climatology, 99,* 187-192.
48. Tabari, H., Paz, S. M., Buekenhout, D., & Willems, P. (2021). Comparison of statistical downscaling methods for climate change impact analysis on precipitation-driven drought. *Hydrology and Earth System Sciences, 25*(6), 3493-3517.
49. Ayugi, B., Zhihong, J., Zhu, H., Ngoma, H., Babaousmail, H., Rizwan, K., & Dike, V. (2021). Comparison of CMIP6 and CMIP5 models in simulating mean and extreme precipitation over East Africa. *International Journal of Climatology, 41*(15), 6474-6496.
50. Dosio, A., Jury, M. W., Almazroui, M., Ashfaq, M., Diallo, I., Engelbrecht, F. A., ... & Tamoffo, A. T. (2021). Projected future daily characteristics of African precipitation based on global (CMIP5, CMIP6) and regional (CORDEX, CORDEX-CORE) climate models. *Climate Dynamics, 57*(11), 3135-3158.
51. Wang, H. M., Chen, J., Xu, C. Y., Zhang, J., & Chen, H. (2020). A framework to quantify the uncertainty contribution of GCMs over multiple sources in hydrological impacts of climate change. *Earth's Future, 8*(8), e2020EF001602.